Published in ApJ. 585, 1114 (2003 March 10)

"Hot Spots" for Solar Flares Persisting for Decades: Longitude Distributions of Flares of Cycles 19–23

T. Bai

Stanford University, Stanford, CA 94305

bai@quake.stanford.edu

ABSTRACT

A new analysis method is introduced for investigating whether major flares are clustered in certain fixed regions of the Sun in rigidly-rotating coordinate systems. This method is applied to analysis of major flares of solar cycles 19–23. Northern and southern hemispheres are separately analyzed, and it is found that longitude distributions of flares in the two hemispheres are different. Therefore, the term "hot spot" is used instead of "active longitude." Seven hot-spot systems are found to be significant, with their rotation periods ranging from 25 to 29 days. Four of them are single-hot-spot systems, and the remaining three are double-hot-spot systems. A double-hot-spot system is made of two hot spots that rotate with the same period but are separated by about 180° in longitude. The most significant hot-spot system is the double-hot-spot system with a period of 26.73 days that operated in the northern hemisphere during cycles 20 and 21. It was previously detected by analysis of flare data of cycles 20 and 21. Now it is found that the prominent hot spot of this system was active during cycle 22. Another double-hot-spot system (with a period of 27.41 days) is found to be in operation in the northern hemisphere during solar cycles 19–21. Another interesting hot-spot system is a single hot spot with a rotation period of 27.0 days, which operated in the northern hemisphere during cycle 21. This hot spot may have the same cause as the 27.03 day periodicity observed in solar wind speed and interplanetary magnetic field. During cycle 23, a double-hot-spot system with a rotation period of 28.2 days is detected in the southern hemisphere but none are detected in the northern hemisphere.

Subject headings: Sun: activity—Sun: flares—Sun: rotation—Sun: interior

1. Introduction

The latitude distribution of sunspots is well known: Sunspots appear mainly in the activity belt, which ranges from 40°S to 40°N. It is curious how sunspots and other solar activity indicators are distributed in longitude. In the 1960s and the early 1970s, several researchers studied whether solar activity occurs preferentially in certain longitude intervals (Trotter & Billings 1962; Warwick 1965; Wilcox & Schatten 1967; Haurwitz 1968; Fung et al. 1971).

In order to define solar longitude, one has to adopt a rotation period of the Sun. Initially, researchers adopted the Carrington longitude for studying distributions of solar activity (Trotter & Billings 1962; Warwick 1965). Such analyses implicitly assume that active longitudes rotate with the Carrington period (sidereal: 25.38 d; synodic: 27.275 d). Since we do not know the rotation period of active longitudes *a priori* even if they exist, we should analyze longitude distributions of solar activity by taking the rotation period as a free parameter, as Wilcox & Schatten (1967) did in re-analyzing the proton flares of Warwick (1965). Haurwitz (1968) analyzed Warwick's proton flares together with important historical flares, taking the rotation period as a free parameter.

Dodson & Hedeman (1968, 1975a), Svestka (1968), and Svestka & Simon (1969) studied active longitude by plotting important active regions in stackplots. These studies have two weak points. First, the data coverage durations for their studies were not long enough—only of order of a few years. Second, their studies did not analyze the statistical significance of "active longitude bands."

Bogart (1982) studied active longitudes by calculating auto-correlation of daily sunspot numbers. Because daily sunspot numbers have no positional information, such analysis can be useful when there is one active longitude band. If there are two active longitude bands separated by 180° in longitude, one of them would be always in the visible hemisphere.

Although many papers were written on active longitudes during the 1960s and 1970s, except for Wilcox & Schatten (1967), Haurwitz (1968), and Fung et al. (1971), they were not quantitative studies because computers were not widely available then. Wilcox & Schatten (1967) re-analyzed Warwick's proton flares produced by 45 active regions and additionally analyzed 745 major flares observed during cycle 19. For each synodic rotation period which varied in the range from 25 to 34 d, Wilcox & Schatten divided the Sun into two hemispheres by two meridians 180° apart such that the "active hemisphere" contains the largest possible number of flares and the other the least number of flares. By doing so, they studied the contrast between the active hemisphere and the inactive hemisphere as a function of rotation period. The hemispheric contrast of the proton flare distribution was

found to be the largest for a period of 28.85 d. For the major flares they analyzed, the hemispheric contrast was the largest for periods of 28.9 d and 30.9 d.

Fung *et al.* analyzed 1,119 flares with Hα class ≥ 2 observed during cycle 19. They used the maximum likelihood method by adopting $f(l) = 1 + A\cos(l - l_0)$ as a trial distribution function, where l is the longitude, l_0 the phase angle, and A the amplitude of modulation. They found that the likelihood was the largest for P=28.80 d. Thus, the two early papers that quantitatively analyzed cycle 19 flares agree that the longitude distributions of flares are the least uniform in a coordinate system rotating with a synodic period of about 28.8 d. This was confirmed by my previous analysis (Fig. 3 of Bai 1988). (In this paper, rotation periods are synodic periods unless specified otherwise.)

By adding for his analysis important historical flares going back to Carrington's white-light flare to the proton flares of Warwick (1965), Haurwitz (1968) implicitly assumed that the longitude distribution was stable for almost 100 years. This assumption has been disproved by Bai (1988). Therefore, his result is not discussed further.

There is no *a priori* reason to assume that the both hemispheres have similar longitude distributions. Fung et al. (1971), who analyzed cycle 19 major flares, showed that the signal for the 28.8-d rotation was mainly due to northern hemisphere flares. During cycle 19, the northern hemisphere produced about two times more major flares than the southern hemisphere. Hence, the hot spot in the northern hemisphere gave rise to a strong signal in the analyses of flares from both hemispheres. My studies (Bai 1987, 1988) also show longitude distributions of flares are different for different hemispheres.

This subject began to get attention again due to the discovery of the 154-d periodicity in solar flare occurrence (Rieger et al. 1984). If two active longitude bands or hot spots have slightly different rotation periods so that they overlap once per 154 d, their interaction might enhance flare activity, causing the 154-d periodicity. In order to test this idea, one should first determine the existence of hot spots (or active longitudes). For this purpose, I analyzed the longitude distribution of major flares observed by the *Solar Maximum Mission (SMM)* during the period from February 1980 to August 1985 and found that about 40 % of the northern-hemisphere major flares were concentrated in a 30° interval in a coordinate system rotating with a synodic period of 26.75 d (Bai 1987). The idea that the 154-d periodicity might be due to interaction of hot spots, which stimulated studies on hot spots, was disproved by Bai & Sturrock (1987).

In a later analysis (Bai 1988), I included major flares selected from the compilations made by Dodson & Hedeman (1971, 1975b, 1981) for the period from 1955 through 1979, in addition to the major flares observed by *SMM*. This study showed that, during cycles

20 and 21, double hot spots rotating with the same period of 26.72 d were in operation in the northern hemisphere. The locations of the double hot spots remained the same during cycles 20 and 21 in a coordinate system rotating with a period of 26.72 d. By calculating the variance of the longitude distribution of sunspot area for the northern hemisphere as a function of rotation period for cycle 21, Akioka et al. (1992) found the largest peak at 26.74 d, in agreement with the study of major flares.

Bai (1990) extended study on hot spots to the early part of cycle 22, selecting flares with GOES (Geostationary Operational Environmental Satellite) class $\geq M3.0$ for cycles 21 and 22, while using CFI major flares for cycle 20, because *SMM* was deorbited in 1989 November. The prominent hot spot of the double-hot-spot system rotating with a period of 26.72 d was found to remain active during the early part of cycle 22. Comparing the results of Bai (1988) and Bai (1990), one can find that the longitude distributions of cycle 21 are independent of major flare selection criteria.

In the 1960s and 70s, the term "active longitude" was used to express a region of frequent flare activity, and it is well known in the solar physics community. This term, however, implies that the northern and southern hemispheres are active in the same longitude band. I began to use the term "hot spot" because the northern and southern hemispheres behave differently in flare clustering (Bai 1988). There is some possibility that this term may be interpreted as an area of higher temperature, but it is a generic term. In international politics, a hot spot means a country or area of frequent conflicts, revolutions, or wars; in geology, it means a region of frequent volcanic activity due to a molten rock in the mantle below such as the Hawaiian hot spot. Therefore, it seems acceptable to use this term, with a modifying phrase attached like "hot spot for solar flares" when necessary.

The plan of this paper is as follows. In §2, I introduce a random-walk analysis method for analyzing longitude distributions of flares. In this method, it is easy to evaluate statistical significances of a single hot spot and double hot spots separated by 180°. In §3 are shown the results of applications of this method to flare data of solar cycles 19–23. Because of the same analysis method, it is easier to compare statistical significances of different hot spot systems detected in different cycles. Analysis of flares of the later part of cycle 22 and of cycle 23 are new because the last analysis (Bai 1990) included flares observed until 1990 April 30. In §4, longitude distributions of flares are discussed. §5 provides summary and discussions.

2. Data and Analysis Methods

2.1. Selection criteria for major flares

For cycles 19 and 20, I use flares compiled by Dodson & Hedeman (1971, 1975b, 1981). They compiled important flares with indices in the following five aspects of flares: Hα importance, ionizing radiation, magnitude of 10-cm radio flux, dynamic radio spectrum, and magnitude of $\sim$200 MHz flux. The sum of these indices of a flare is defined as its CFI (comprehensive flare index). For cycle 19, a major flare is defined as a flare with a CFI ≥ 5; for cycle 20, a major flare is defined as a flare with a CFI ≥ 6. A lower threshold is used for cycle 19 because observations for determining CFIs were less complete during cycle 19.

For cycles 21–23, flares with GOES soft X-ray classes $\geq$M3.0 (peak X-ray flux in the 1–8 $\mathring{A}$ band $\geq 3.0 \times 10^{-5}\ Wm^{-2}$) are selected. Flare data are obtained from the Geophysical Data Center of the National Oceanic and Atmospheric Administration.

Table 1 shows the numbers of major flares with their active regions identified and the the numbers of active regions producing major flares by cycles and hemispheres. Flare data for cycle 23 include observations made until 2002 June 20. The number of major flares is not large for cycle 19 even though it was the strongest cycle, because the selection criterion for major flares for cycle 19 is different from those for other cycles.

2.2. Analysis methods

Suppose that there is a set of events with angular values $\{\theta_1, \theta_2, \theta_3, \cdots, \theta_N\}$. There are several method of testing whether these events have a uniform angular distribution or they are concentrated in a certain angular interval. In my previous papers (Bai 1987, 1988, 1990), I calculated the r.m.s. deviation of the longitude distribution as a function of rotation period. This method finds rotation periods for which longitude distributions of flares are far from being uniform. Similarly, Akioka et al. (1992) calculated the variance of longitude distribution of sunspots as a function of rotation period. However, in this method, it is not straightforward to calculate statistical significance.

Jetsu & Pelt (1996) developed a periodicity analysis method of a weighted time point series, and Jetsu et al. (1997) applied it to analysis of central meridian passage times of superactive regions (Bai 1988) by weighting with their number of major flares. They confirmed the double hot system with a rotation period of 26.72 d.

In the Rayleigh analysis, one examines the event distribution on a unit circle with its

center at the origin of an X-Y plane (a two-dimensional parameter space), where angles are measured from the X-axis. Then, each event can be expressed as a unit vector, $\vec{u}_i = \vec{e}_x \cos\theta_i + \vec{e}_y \sin\theta_i$, where $\vec{e}_x$ and $\vec{e}_y$ are unit vectors parallel to the X and Y axes, respectively, and θ_i is the angle of the ith event. The vector sum of these unit vectors,

$$\vec{R} = \vec{e}_x \sum_{i=1}^{N} \cos\theta_i + \vec{e}_y \sum_{i=1}^{N} \sin\theta_i \tag{1}$$

represents the character of the angular distribution (see Mardia 1972, pp. pp. 131–136). We find this problem is the same as a random walk problem, if we regard the unit vector of the ith event $\vec{u}_i$ as the ith step of a random walker. The vector $\vec{R}$ corresponds to the total displacement from the origin of the random walker. The expectation value of the square of this vector R^2 is proportional to the number N, if the directions of unit vectors are random. Thus, the probability for R^2/N to be greater than a by chance is

$$F(R^2/N \geq a) = e^{-a}. \tag{2}$$

In order to investigate whether events are concentrated in two angular intervals separated by 180°, the following vector is used instead of the vector given by equation (1):

$$\vec{R} = \vec{e}_x \sum_{i=1}^{N} \cos 2\theta_i + \vec{e}_y \sum_{i=1}^{N} \sin 2\theta_i. \tag{3}$$

We can apply this method to investigation of longitude distributions of flares, by substituting longitudes of flares into θ_i in equation (1). Since longitudes of flares depend on the rotation period of the coordinate system, the function

$$z(P) = \frac{R^2}{N} = \frac{1}{N}\left[\left(\sum_{i=1}^{N} \cos\theta_i\right)^2 + \left(\sum_{i=1}^{N} \sin\theta_i\right)^2\right] \tag{4}$$

can be regarded as a power spectrum as a function of the rotation period. If flares are concentrated in a certain longitude interval in a coordinate system rotating with a period P_1, $z(P)$ will show a prominent peak at $P = P_1$, and the probability of finding such a peak at $P = P_1$ by chance will be $\exp\{-z(P_1)\}$. This is the so-called Rayleigh analysis method, which has been used in flare periodicity analyses by Dröge et al. (1990) and Bai & Cliver (1990).

In the above discussion, it is assumed that events are statistically independent from each other. However, some active regions produce several major flares, and the longitudes of major flares from the same active region are not random but similar to each other. In what follows an attempt is made to take this into consideration.

Let us define $\vec{R}_j$ as the vector sum of all unit vectors corresponding to major flares from the active region number j:

$$\vec{R}_j = \vec{e}_x \sum_{k=1}^{n_j} \cos\theta_{jk} + \vec{e}_y \sum_{k=1}^{n_j} \sin\theta_{jk} \tag{5}$$

where n_j is the number of major flares from the active region number j, and θ_{jk} is the longitude of the kth major flare from the active region number j.

Now we have to evaluate whether the vectors $\vec{R}_j$ are randomly distributed or not. This is just a random walk problem with varying step sizes. Thus, we should consider the magnitude of the total displacement vector, the r.m.s. step size, and the total number of steps. The displacement vector is given by

$$\vec{R} = \sum_{j=1}^{n} \vec{R}_j \tag{6}$$

where n is the number of active regions producing major flares, corresponding to the number of steps. The r.m.s. step size is given by

$$S = \sqrt{\sum_{j=1}^{n} R_j^2/n}. \tag{7}$$

The probability for z_{nor} greater than z_0 by chance is $\exp(-z_0)$, if we define z_{nor} as

$$z_{nor} = \frac{1}{n}(R/S)^2 = \frac{\left(\sum_{j=1}^{n} \vec{R}_j\right)^2}{\sum_{j=1}^{n} R_j^2}. \tag{8}$$

Rewriting this equation, we get

$$z_{nor}(P) = \frac{\left(\sum_{j=1}^{n}\sum_{k=1}^{n_j} \cos\theta_{jk}\right)^2 + \left(\sum_{j=1}^{n}\sum_{k=1}^{n_j} \sin\theta_{jk}\right)^2}{\sum_{j=1}^{n}\left(\sum_{k=1}^{n_j} \cos\theta_{jk}\right)^2 + \sum_{j=1}^{n}\left(\sum_{k=1}^{n_j} \sin\theta_{jk}\right)^2}. \tag{9}$$

This equation provides a properly normalized power spectrum as a function of rotation period P.

The above equation is good for detecting a single hot spot. To detect double hot spots, which have the same rotation period but are separated by 180°, we should investigate bimodal distribution by changing θ_{jk} in the above equation into $2\theta_{jk}$. Thus, the normalized power spectrum for double hot spots is given by

$$z_{nor}(P) = \frac{\left(\sum_{j=1}^{n}\sum_{k=1}^{n_j}\cos 2\theta_{jk}\right)^2 + \left(\sum_{j=1}^{n}\sum_{k=1}^{n_j}\sin 2\theta_{jk}\right)^2}{\sum_{j=1}^{n}\left(\sum_{k=1}^{n_j}\cos 2\theta_{jk}\right)^2 + \sum_{j=1}^{n}\left(\sum_{k=1}^{n_j}\sin 2\theta_{jk}\right)^2}. \tag{10}$$

After calculating a power spectrum, one has to calculate the significance of a peak in the spectrum. The false alarm probability (FAP) is defined as the probability of finding by chance a peak with a value of z_0 in the search window (Scargle 1982). It is calculated by

$$FAP = 1 - [1 - \exp(-z_0)]^m \,. \tag{11}$$

Here m is the number of independent frequencies, which is calculated by

$$m = \frac{f_2 - f_1}{f_{ind}} \tag{12}$$

where f_1 and f_2 are the lower and upper limit frequencies of the search window, and f_{ind} is the independent frequency spacing.

For an evenly sampled time series, $f_{ind} = 1/T$, where T is the total time interval. Even for a time point series, the same f_{ind} can be used because spectral resolution depends only on T. In this paper, I analyze spectra in the rotation period interval 24–30 d. For single hot spot analysis, this interval corresponds to the frequency interval 385.8–482.3 nHz. (Numerically, a rotation period P and its frequency f are related by $f = 11,574/P$, when f and P are in units of nHz and d, respectively.) For double hot spot analysis, the corresponding frequency interval is 771.6–964.5 nHz because the passage of a hot spot through the central meridian occurs twice per rotation. We can see the doubling of independent frequencies for double-hot-spot systems by comparing the variations of power in the lower panel with those in the upper panel of Figure 2, for example.

The formula for FAP simplifies to

$$FAP \simeq m \exp(-z_0), \tag{13}$$

if $\exp(-z_0) \ll 1$.

In order to test whether the power spectra defined by equations (9) and (10) are properly normalized, I have done the following. First, I have calculated the powers defined by equation (10) at 1.5 nHz intervals in the range 330–579 nHz (corresponding to the 20–35 d range) for northern-hemisphere flares of cycle 21. Here 1.5 nHz is the independent frequency spacing for double-hot-spot systems. The resulting 166 power values are sorted to see the distribution of power values. Second, I have performed Monte Carlo simulations to shuffle the occurrence times of northern-hemisphere flares of cycle 21, requiring the following three conditions. (1) The long-term flare rate should follow the 100-d running mean of the actual flare production rate of cycle 21. (2) The flares from the same active region should move as a group, maintaining their relative timing. (3) The flare locations on the disk should be the same as the actual locations. For each set of simulated flare data, I have calculated powers at 166 frequencies explained above. I have made 10 simulations and sorted the resulting 1,660 values of power to see the distribution of powers.

In Figure 1, it is shown in how many cases power exceeds certain values. The top part of the figure (made of small dots and crosses) shows the result for simulated cases. The result conforms very well to the normalized exponential distribution shown by the upper straight line. This proves that the power spectrum defined by equation (10) is properly normalized. The lower part of the figure (made of small dots and asterisks) shows the result for the actual flare data. For low values of power, the distribution follows very well the normalized exponential distribution, shown by the lower straight line. The two highest values of power are due to two double-hot-spot systems, respectively (cf. Fig. 4). (For the results shown in Figure 1, I have calculated powers in the 20–35 d interval to have a large number of independent frequencies. For the results to be shown in the next section, I calculate powers in the rotation period interval from 24 to 30 d.)

I have performed a similar test for the power spectrum defined by equation (9), for single-hot-spot systems. The results are as satisfactory as the above.

As seen in this section, it is simple to calculate normalized Rayleigh power spectra for angular distributions. It is also straightforward to calculate the statistical significances of the peaks in the spectra. Therefore, I am going to use this method in this paper.

3. Spectral Analysis Results

3.1. Cycle 19

Figure 2 shows power spectra for longitude distributions of major flares for cycle 19. The only prominent peak is at 28.88 d for a single hot spot in the northern hemisphere.

This period is consistent with the periods found by Wilcox & Schatten (1967) and Fung et al. (1971), and this figure confirms that the signal mainly comes from northern hemisphere flares (Fung et al. 1971).

The search window in this study is the rotation period interval from 24–30 d, which corresponds to the 386–482 nHz frequency interval. T is 3681 d (1955 Jan 1 – 1965 Feb 28). The FAP for $m = 31$ and $z_0 = 9.93$ is 1.50×10^{-3}. In other words, the 28.88-d peak is significant at the 99.85% level.

3.2. The northern hemisphere of cycles 19–21

Figure 3 shows power spectra for single hot spot systems. The peak at 27.0 d in the spectrum for cycle 21, whose value is 7.28, is statistically significant ($FAP = 0.015$). By analyzing solar wind speed and interplanetary magnetic field, Neugebauer et al. (2001) found a 27.03-d periodicity. This periodicity may have the same cause as the 27.0-d hot spot.

Figure 4 shows power spectra for double-hot-spot systems for flares of cycles 20 and 21. In the spectra for cycle 20, two big peaks are at 26.73 d and 27.44 d. In the spectra for cycle 21, two big peaks are at 26.70 d and 27.35 d. In the spectrum for the two cycles combined, the peaks at 26.73 d and 27.41 d are very prominent. In the spectrum for cycles 19–21 (not shown here), the height of the 26.73-d peak is smaller than the same peak in Figure 4a, but the 27.41-d peak has a value as large as 13.21. This means that the double-hot-spot system with a rotation period of 26.73 d persisted in the same locations during cycles 20 and 21, and the double-hot-spot system with a rotation period of 27.41 d persisted in the same locations during the three solar cycles. (This will be shown in Figure 13.)

3.3. The southern hemisphere of cycles 19–21

Figure 5 shows power spectra for single-hot-spot systems for southern hemisphere flares of cycles 19 and 20. In the spectrum for cycle 20, a very prominent peak is found at 24.98 d, with a peak value of 9.08. The FAP of this peak is 0.4% (for $m = 35$).

In the both spectra for cycles 19 and 20, a peak at 28.00 d is found although their peak values are not high. However, in the spectrum for the combined data of the two cycles, this peak stands out with a peak value of 7.93. This means that the hot spot with a rotation period of 28.00 d persisted at the same location during the two cycles. The FAP of this peak is 2.3% (for $m = 66$).

The power spectrum for single-hot-spot systems for southern hemisphere flares of cycle 21 is not shown here because there is no significant peak.

Let us study double-hot-spot systems for southern hemisphere flares of cycles 20–22. Figure 6 shows spectra for southern double-hot-spot systems for cycles 21 and 22 separately and combined. The spectrum for cycle 22 and the spectrum for cycles 21 and 22 are shown here because the 25.09-d peak in the spectrum for cycle 21 becomes bigger in the spectrum for both cycles. The power spectrum for cycle 20, on the other hand, is not shown here because there is no significant peaks. The peak at 25.09 d in the spectrum of the combined data has a value of 7.30. Its FAP is 0.08 (for $m = 123$). This periodicity is, therefore, significant only at the 92% confidence level.

3.4. Cycle 22

Figure 7 shows spectra for cycle 22. There is no significant peaks in any of the four spectra shown here. Cycle 22 seems exceptional, compared with other cycles.

3.5. Cycle 23

Figure 8 shows power spectra for longitude distributions for cycle 23. The only peak worth mentioning is found at 28.24 d in the spectrum for double-hot-spot systems in the southern hemisphere. The peak value is 7.74, and its FAP is estimated to be 1.5%.

4. Longitude Distributions

In this section, let us study longitude distributions of flares for chosen hot-spot systems.

Figure 9 shows longitude distributions of flares in a coordinate system rotating with a 28.00-d period for cycles 19 and 20, separately. The central meridian at the beginning of 1955 is taken as the zero longitude. Flares are enhanced in the longitude interval from 140° to 300°. The flare enhancement indicated by a in the lower panel and the flare enhancement indicated by b in the upper panel appear in the same longitude band, if we adopt a coordinate system rotating with a period of 27.99 d. In such a coordinate system, the longitude distribution of southern hemisphere flares of cycle 21 also shows enhancement in the same longitude interval (cf. Bai 1988).

Figure 10 shows the longitude distribution of southern-hemisphere flares of cycle 20 in

a coordinate system rotating with a 24.98-d period. The central meridian at the beginning of 1965 is taken as the zero longitude. Enhancement of flares in the 300–400° interval is impressive.

Figure 11 shows the longitude distribution of northern-hemisphere flares for cycle 21 in a coordinate system rotating with a 27.0-d period. The central meridian at the beginning of 1976 is taken as the zero longitude. The distribution resembles a sinusoidal curve, instead of having a sharp peak. This is probably the reason that this hot spot was not detected in an analysis calculating r.m.s. values of the longitude distribution (cf. Bai 1988).

Figure 12 shows longitude distributions of northern-hemisphere flares for cycles 20, 21, and 22, respectively, in a coordinate system rotating with a period of 26.73 d. The central meridian at the beginning of 1965 was taken as the zero longitude. During cycle 20, two hot spots are separated by about 180°. The prominent hot spot centered around 130° remained at the same location through the three cycles. The less prominent hot spot, on the other hand, became closer to the prominent hot spot during later cycles. The separation between the two hot spots was $\sim 160°$ during cycle 21 and only $\sim 130°$ during cycle 22. The bimodal power described in equation (10) is large when two hot spots are separated by 180°. This is why the power spectrum for northern-hemisphere flares of cycle 22 does not show any noticeable peak near 26.73 d even though the longitude distribution for this rotation period shows a prominent hot spot.

In order to test whether the similarity between the longitude distributions of cycles 21 and 22 for the period 26.73 is due to chance, I have calculated the following cross correlation function:

$$C = \frac{1}{360} \prod_{\theta=1}^{360} f_{21}(\theta; P = 26.73\ d) f_{22}(\theta; P = 26.73\ d) \tag{14}$$

where $f_{21}(\theta; P = 26.73\ d)$ and $f_{22}(\theta; P = 26.73\ d)$ are the longitude distributions of flares of cycles 21 and 22, respectively normalized to have a mean value 1, as a function of longitude θ in a coordinate system rotating with a period 26.73 d. It is found that $C = 1.424$.

In order to evaluate the probability to have such a large value of cross correlation by chance, I have made Monte Carlo simulations to shuffle the occurrence times of northern-hemisphere flares of cycle 22, following the three conditions explained in Section 2. For 3,000 cases, I have calculated longitude distributions of cycle 22 flares in a system rotating with a period of 26.73 d and their cross correlations with the actual flare distribution $f_{21}(\theta; P = 26.73\ d)$. Only 16 out of 3,000 cases, the cross correlation function exceeds 1.424. Therefore, the probability that the longitude distribution of cycle 22 northern-hemisphere flares for

$P = 26.73\ d$ looks similar to that for cycle 21 by random chance is only about 0.5%.

Figure 13 shows longitude distributions of northern-hemisphere flares for cycles 19–21 in a coordinate system rotating with a period of 27.41 d. The central meridian at the beginning of 1954 is taken as the zero longitude. The three distributions are similar in showing two longitude intervals of flare enhancement, which are separated by about 180°. These hot spots remained in the same location during the three cycles. However, the distribution for cycle 19 shows additional enhancement in the 140–200°, and the distribution for cycle 21 shows additional enhancement in the 340–40° interval.

Figure 14 shows longitude distribution of southern-hemisphere flares for cycle 22 in a coordinate system rotating with a period of 28.24 d. The central meridian at the beginning of 1997 is taken as the zero longitude. Two hot spots are separated by $\sim 180°$.

5. Summary and Discussion

A random walk problem with varying step sizes is applied to analysis of longitude distribution of major flares. In this method, only simple calculations are required, and it is easy to evaluate statistical significance. Therefore, this method is much better than the methods used previously.

Many hot-spot systems are discussed in this paper. The ones with FAP less than 3% are listed in Tables 2 and 3. The hot spots that have been already discovered by previous studies are indicated by the references in Table 2. Four hot spot systems are newly discovered in this paper.

Uncertainties of rotation periods depend on life times and longitudinal extents of hot spots. The longer the life time, the smaller is the uncertainty. The larger the longitudinal extent, the larger is the uncertainty. Uncertainties also depend on the stability of locations of hot spots. The double-hot-spot system with a rotation period of 26.73 d has the smallest uncertainty, about 0.01 d, and the 27.0-d hot spot has the largest uncertainty, about 0.06 d.

What is the mechanism (or mechanisms) for hot spots? It seems premature to expect to have the answer now. However, the following characteristics of hot spots must be explained by a successful mechanism.

First, life times of some hot spot systems are longer than one solar cycle. It is generally thought that magnetic fields responsible for 11-year cycles are generated at the bottom of the convection zone. Considering that the Hale polarity changes from one 11-year cycle to another, we can deduce that the toroidal magnetic flux tubes for each cycle are newly

generated with old ones being destroyed. Therefore, the mechanism(s) for hot spot systems lasting for more than one solar cycle must be independent of toroidal magnetic flux tubes.

Compared to long life times of hot spots, convective turn-over times are of order of months. Additionally, any structure in the convection zone will be destroyed by differential rotations in a relatively short time, if it participates in differential rotations. For example, a fictitious particle following the rotation rate of 10°N given by Scherrer et al. (1980) will make 14.57 rotations in a year. A fictitious particle following the rotation rate of 25°N will make 14.16 rotations in a year. Therefore, if a structure extending from 10°N to 25°N participates in differential rotations, it will be stretched by 148° in longitude in one year. It may be possible to maintain a long-term coherency in the convection zone because, in turbulent fluids, sometimes long-lasting patterns are observed (Prigogine & Stengers 1989). It would be, however, much easier to maintain their coherency if agencies causing hot spots are in the overshoot region where the rotation is more rigid.

Second, synodic rotation periods of hot spots range from 25 to 29 d. This range surpasses the range of rotation periods observed both on the surface and in the convection zone in the latitude zone from $-35°$ to 35°. These rotation periods are not directly related to rotation periods of individual active regions or activity nests, contrary to Pojoga & Cudnik (2002). The following analogy may be illuminating. If an animal submerged in the river blows out bubbles once in a while, from the times and locations of bubble emergences, one can calculate the speed of the animal. This speed is not necessarily the same as the flow speed of bubbles, which is determined by the surface flow.

Third, hot-spot systems with different rotation periods coexist in the same hemisphere during the same cycle.

Fourth, the northern and southern hemispheres have different hot spots. The mechanism for hot spots should be confined within the hemisphere.

The transportation of magnetic fields from the bottom to the upper part of the convection zone is thought to be mainly due to magnetic buoyancy (Choudhuri & Gilman 1987; Fan et al. 1994). The existence of hot spots indicates that the mechanism for hot spots, whatever it may be, must play a key role in transporting magnetic fields. It is plausible that the hot-spot mechanism operating in the overshoot region where toroidal magnetic flux ropes are generated make initial kinks in the flux ropes, and magnetic bouyancy operates more effectively in the kinked regions.

This research was supported by NSF grant ATM-0102184.

REFERENCES

Akioka, M., Kubota, J., Suzuki, M. and Tohmura, I. 1992, Sol. Phys., 139, 177

Bai, T. 1987, ApJ, 314, 795

Bai, T. 1988, ApJ, 328, 860

Bai, T. 1990, ApJ, 364, L17

Bai, T. 1992, ApJ, 397, 584

Bai, T., & Cliver, E. W. 1990, ApJ, 363 299

Bai, T., & Sturrock, P. A. 1987, Nature, 327, 601

Bogart, R. S. 1982, Sol. Phys., 76, 155

Choudhuri, A. R., & Gilman, P. A. 1987, ApJ, 316, 788

Dodson, H. W., & Hedeman, E. R. 1968, in Structure and Development of Solar Active Regions, IAU Symp. 35, ed. K. O. Kiepenheuer, Dordrecht: Reidel, 56

Dodson, H. W., & Hedeman, E. R. 1971, An Experimental, Comprehensive Flare Indices and Its Derivation for "Major" Flares, 1955-1969, World Data Center for Solar-Terrestrial Physics Report UAG-14, Boulder: NOAA

Dodson, H. W., & Hedeman, E. R. 1975a, Sol. Phys., 42, 121

Dodson, H. W., & Hedeman, E. R. 1975b, Experimental Comprehensive Solar Flare Indices for Certain Flares, 1970-1974, World Data Center for Solar-Terrestrial Physics Report UAG-52, Boulder: NOAA

Dodson, H. W., & Hedeman, E. R. 1981, Experimental Comprehensive Solar Flare Indices for "Major" and Certain Lesser Flares, 1975-1979,World Data Center for Solar-Terrestrial Physics Report UAG-80, Boulder: NOAA

Dröge, W. Gibbs, K., Grunsfeld, J. M., Meyer, P., & Newport, B. J. 1990, ApJS, 73, 279

Fan, Y., Fisher, G. H., & McClymont, A. N. 1994, ApJ, 436, 907

Fung, P. C. W., Sturrock, P. A., Switzer, P. S., & van Hoven, G. 1971, Sol. Phys., 18, 90

Haurwitz, M. W. 1968, ApJ, 151, 351

Jetsu, L., & Pelt, J. 1996, A&AS, 118, 587

Jetsu, L., Pohjolainen, S., Pelt, J., & Tuominen, I. 1997, A&A, 318, 293

Mardia, K. V. 1972, Statistics of Directional Data, New York: Academic Press

Neugebauer, M., Smith, E. J., Ruzmaikin, A., Feynman, J., & Vaughan, A. H. 2001, J. Geophys. Res., 105, 2315

Pojoga, S., & Cudnik, B. 2002, Sol. Phys., 208, 17

Prigogine, I., & Stengers, I. 1989, Order out of Chaos, New York: Doubleday

Rieger, E., Share, G. H., Forrest, D. J., Kanbach, G., Reppin, C., & Chupp, E. L. 1984, Nature, 312, 623

Scargle, J. D. 1982, ApJ, 263, 835

Scherrer, P. H., Wilcox, J. M., and Svalgaard, L. 1980, ApJ, 241, 811

Svestka, Z. 1968, Sol. Phys., 4, 18

Svestka, Z., & Simon, P. 1969, Sol. Phys., 10, 3

Trotter, D. E., & Billings, D. E. 1962, ApJ, 136, 1140

Warwick, C. S. 1965, ApJ, 141, 500

Wilcox, J. M., & Schatten, K. H. 1967, ApJ, 147, 364

This preprint was prepared with the AAS LaTeX macros v5.0.

Table 1: Numbers of Major Flares and Active Regions.

Cycle	N. A.R.[a]	S. A.R.[b]	N. flares	S. flares	N/(N+S) ratio[c](%)
19	136	85	281	148	66
20	114	67	250	117	68
21	114	110	316	318	50
22	93	127	218	334	39
23	62	58	124	108	53

[a]This is the number of northern hemisphere active regions that produced one or more major flares.

[b]This is the number of southern hemisphere active regions that produced one or more major flares.

[c]This is the ratio between the number of northern hemisphere major flares and the total number of major flares from both hemispheres.

Table 2: Hot Spot Systems.

Period (d)	S. or D.	Cycle	Hemisphere	Peak value	$FAP(\%)$	Ref.
28.88	Single	19	N	9.93	0.15	1,2
26.73	Double	20, 21, 22	N	14.05	0.010	3,4
27.0	Single	20	N	7.28	1.5	
27.41	Double	19, 20, 21	N	13.21	0.035	
28.00	Single	19, 20	S	7.93	2.3	3
25.0	Single	20	S	9.08	0.4	
28.24	Double	23	S	7.74	1.5	

References. — (1) Wilcox & Schatten 1968; (2) Fung et al. 1971; (3) Bai 1988; (4) Akioka et al. 1992

Table 3: Hot Spot Systems by Cycles.

Cycle	N. Hemisphere	S. Hemisphere
19	28.88 d (1)	28.00 d (1)
19	27.41 d (2)	
20	27.41 d (2)	28.00 d (1)
20	26.73 d (2)	24.98 d (1)
21	27.0 d (1)	
21	26.73 d (2)	
21	27.41 d (2)	
22	26.73 d (2)	
23		28.2 d (2)

[a]Numbers in parentheses indicate hot spot numbers in the hot spot systems.

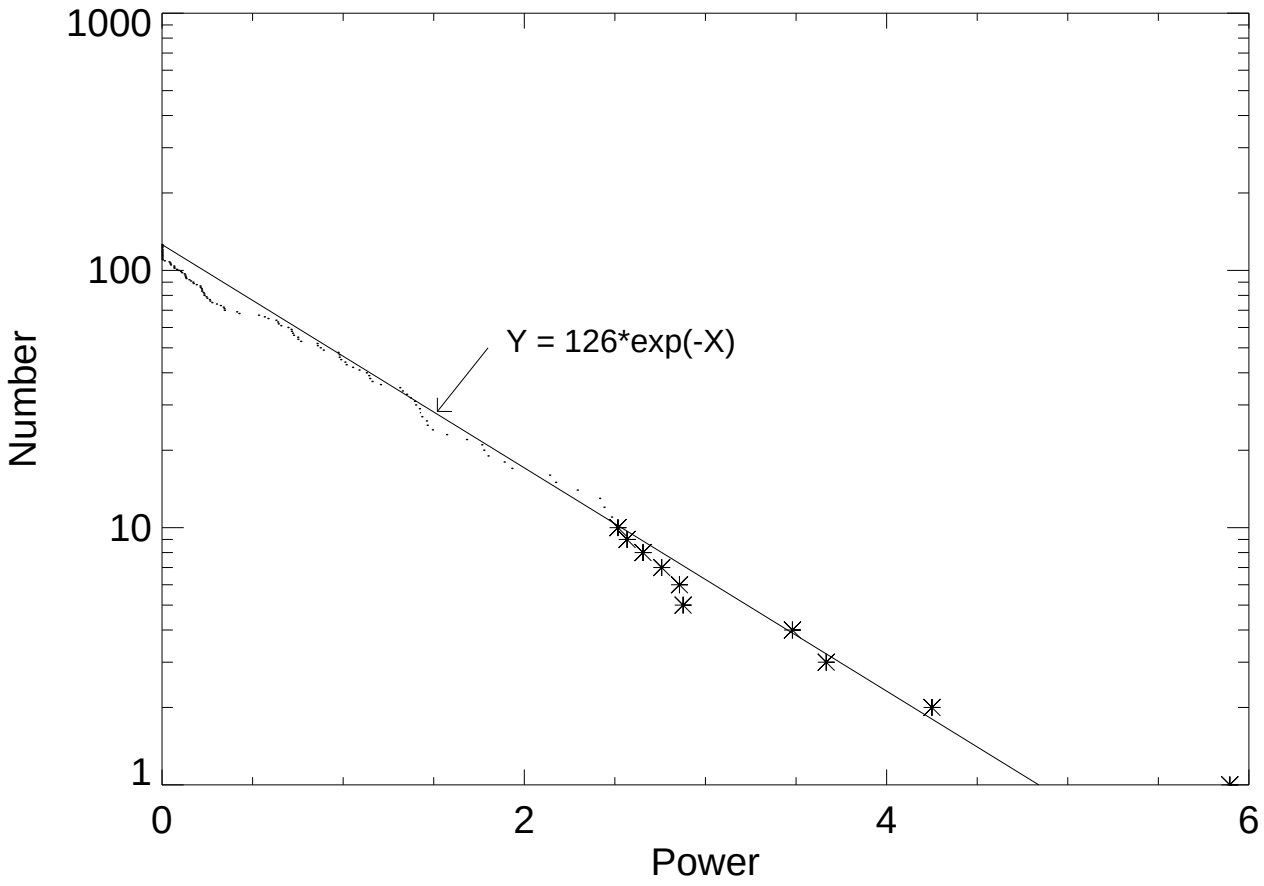

Fig. 1.— Distribution of Powers. The number of cases where powers are equal to or greater than a certain value is plotted as a function of power. It is explained in the text how the powers are calculated. For low values of power, results are shown by small dots because they are crowded. For high values of power, results are shown by big symbols to make them more visible. The two straight lines are normalized exponential distribution indicated by the two equations in the figure.

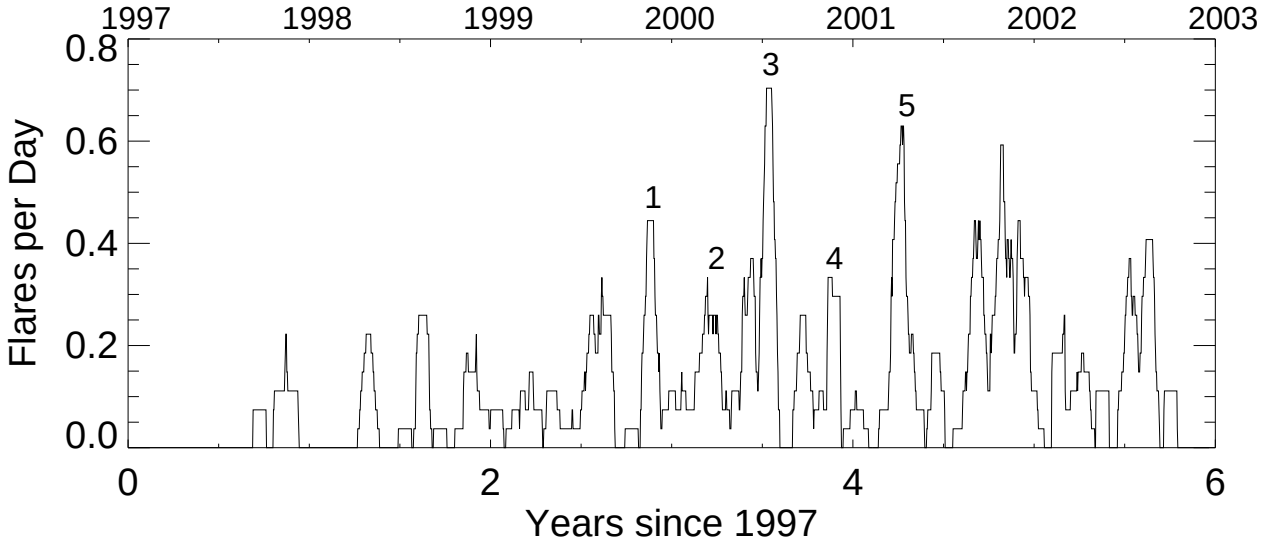

Fig. 2.— Power spectra for cycle 19. Power spectra shown in the upper panel is shifted upward by adding 10. Similar shifts are made for Figs. 3–8. Dotted horizontal lines in this figure indicate the level for $FAP = 10\%$; dashed horizontal line, $FAP = 1\%$; dash-dotted line, $FAP = 0.1\%$. The same convention is used for Figs. 3–8. Only the 28.88-d peak is significant.

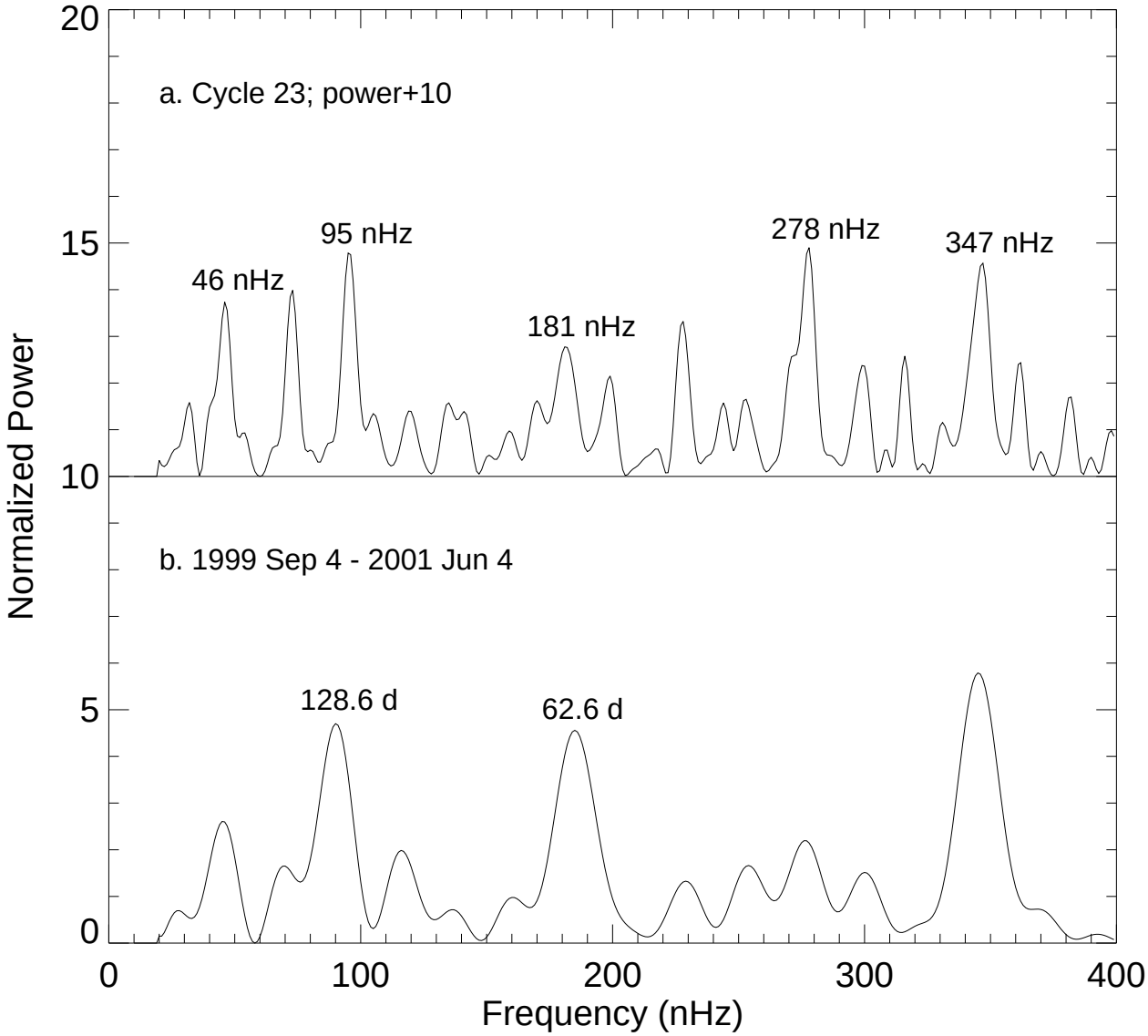

Fig. 3.— Power spectra for northern-hemisphere flares of cycles 20 and 21 for single hot spots.

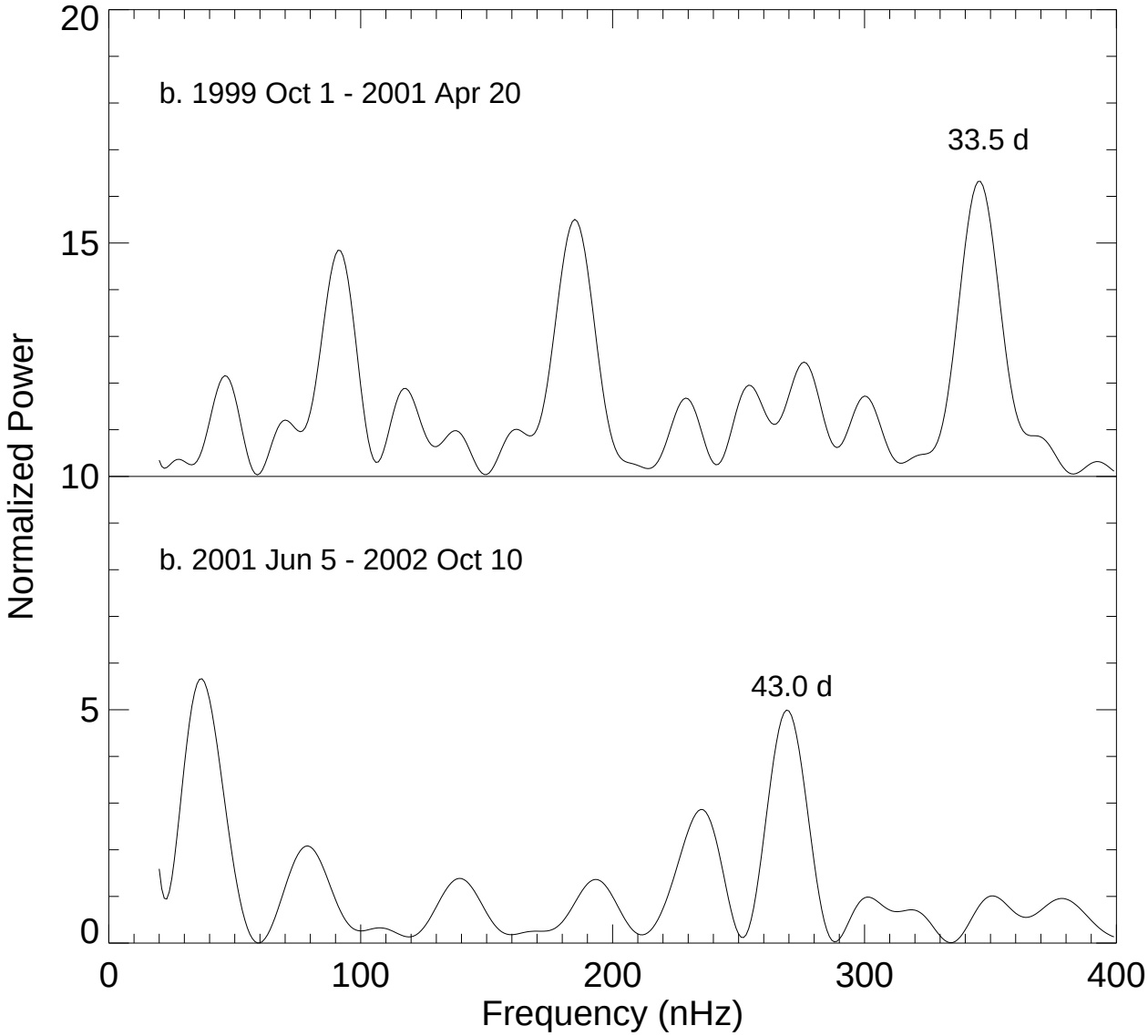

Fig. 4.— Power spectra for northern-hemisphere flares of cycles 20 and 21 for double hot spots.

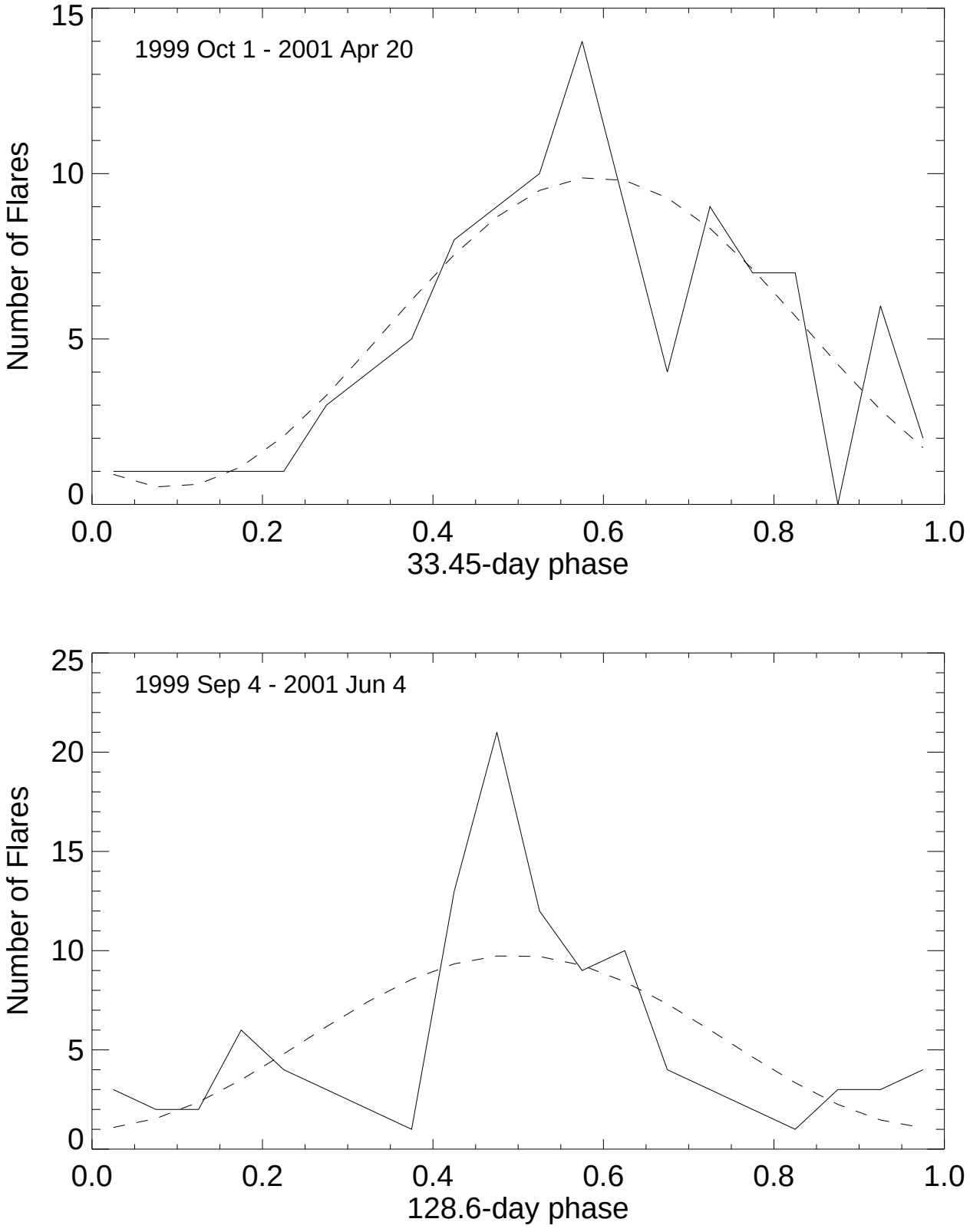

Fig. 5.— Power spectra for southern-hemisphere flares of cycles 19 and 20 for single hot spots.

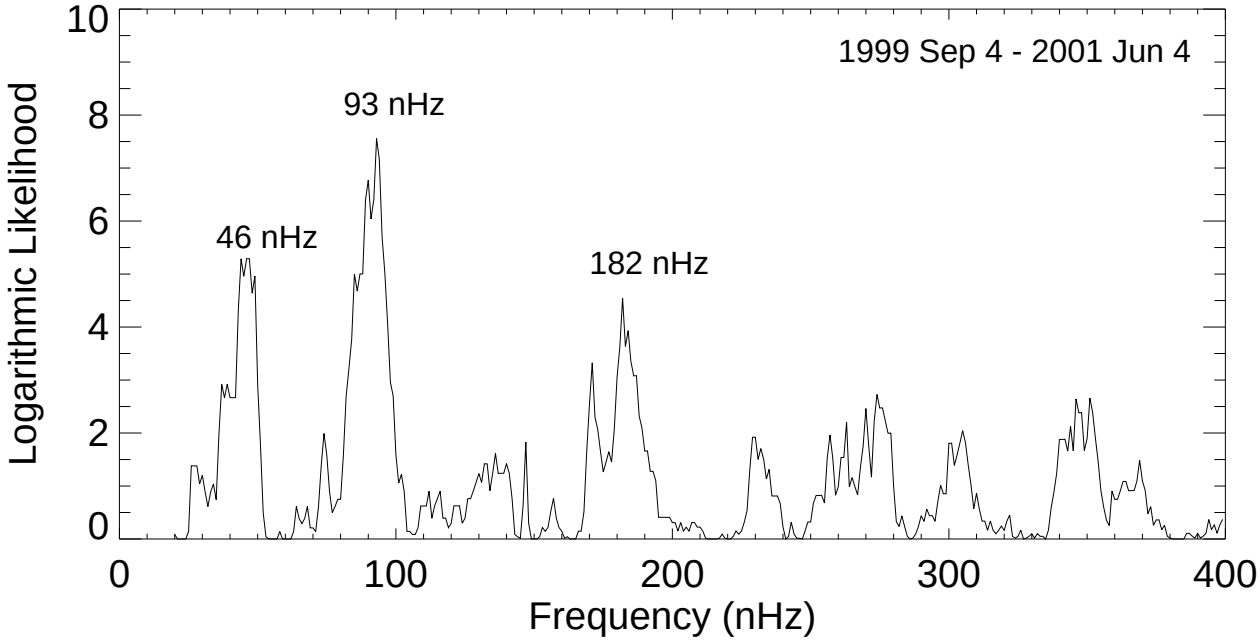

Fig. 6.— Power spectra for southern-hemisphere flares of cycles 21 and 22 for double hot spots.

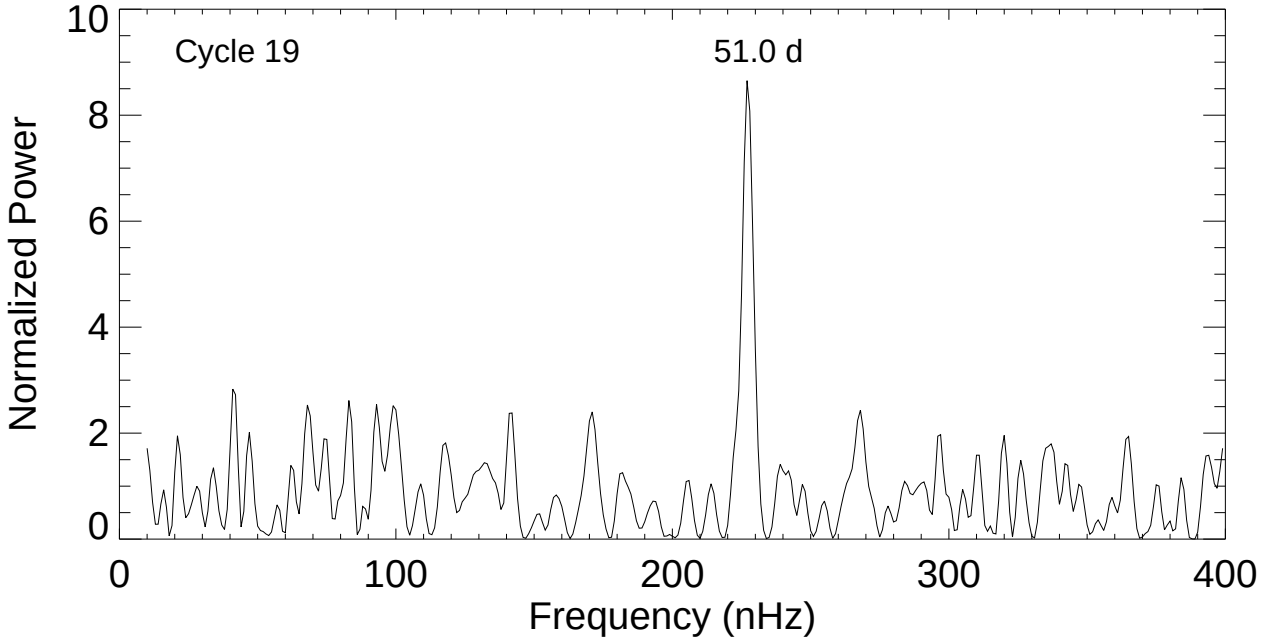

Fig. 7.— Power spectra for cycle 22.

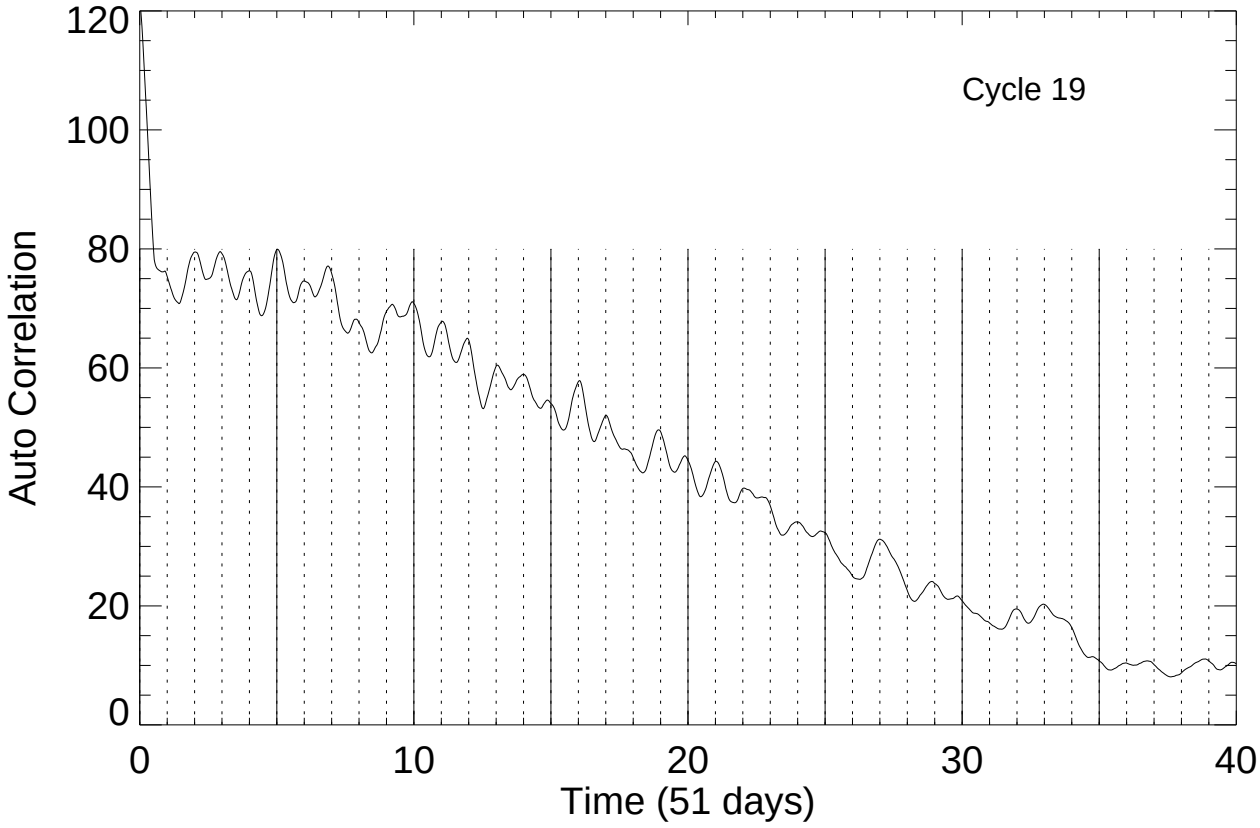

Fig. 8.— Power spectra for cycle 23. A double-jot-spot system with $P = 28.24\,d$ is significant.

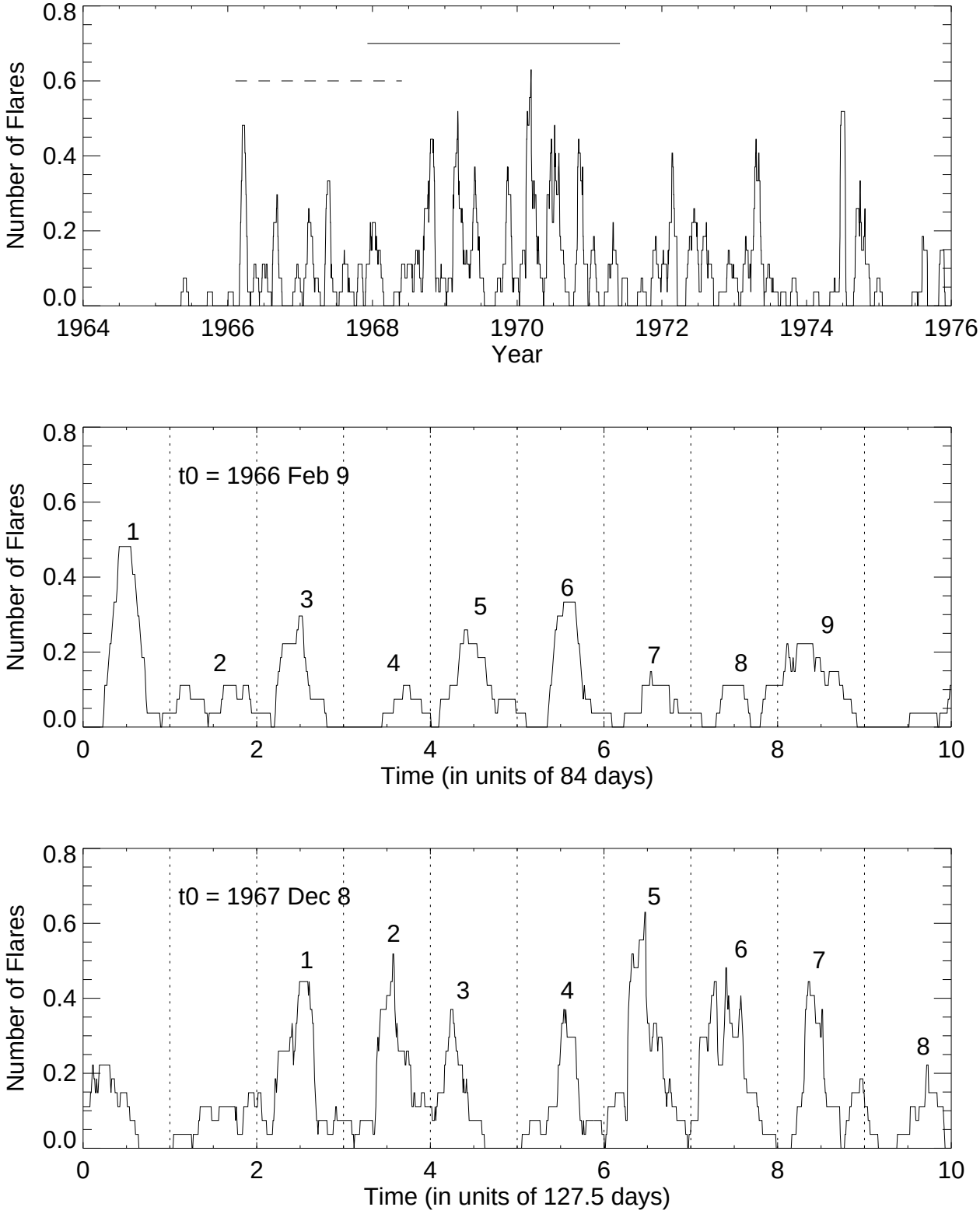

Fig. 9.— Longitude distributions for southern-hemisphere flares of cycles 19 and 20 for $P = 28.00$ d. The values for the 360–400° interval are the same as those for the 0–40° interval. The 360–400° interval is added to show the continuation of the distribution. In this figure and other figures showing longitude distributions, the number of flares in a 30° interval is plotted. The baseline for the upper panel is $y = 50$.

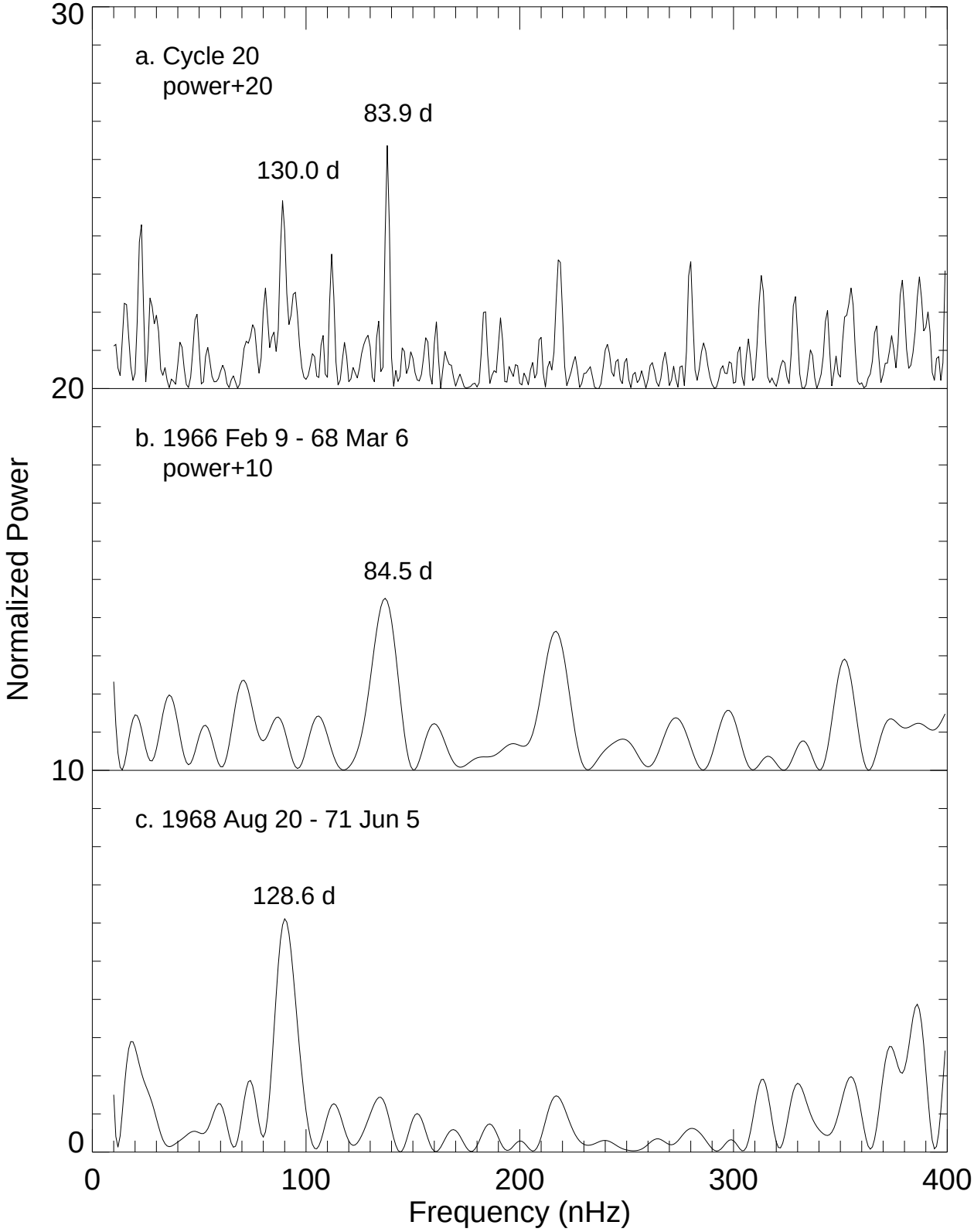

Fig. 10.— Longitude distribution for southern-hemisphere flares of cycle 20 for $P = 24.98\ d$.

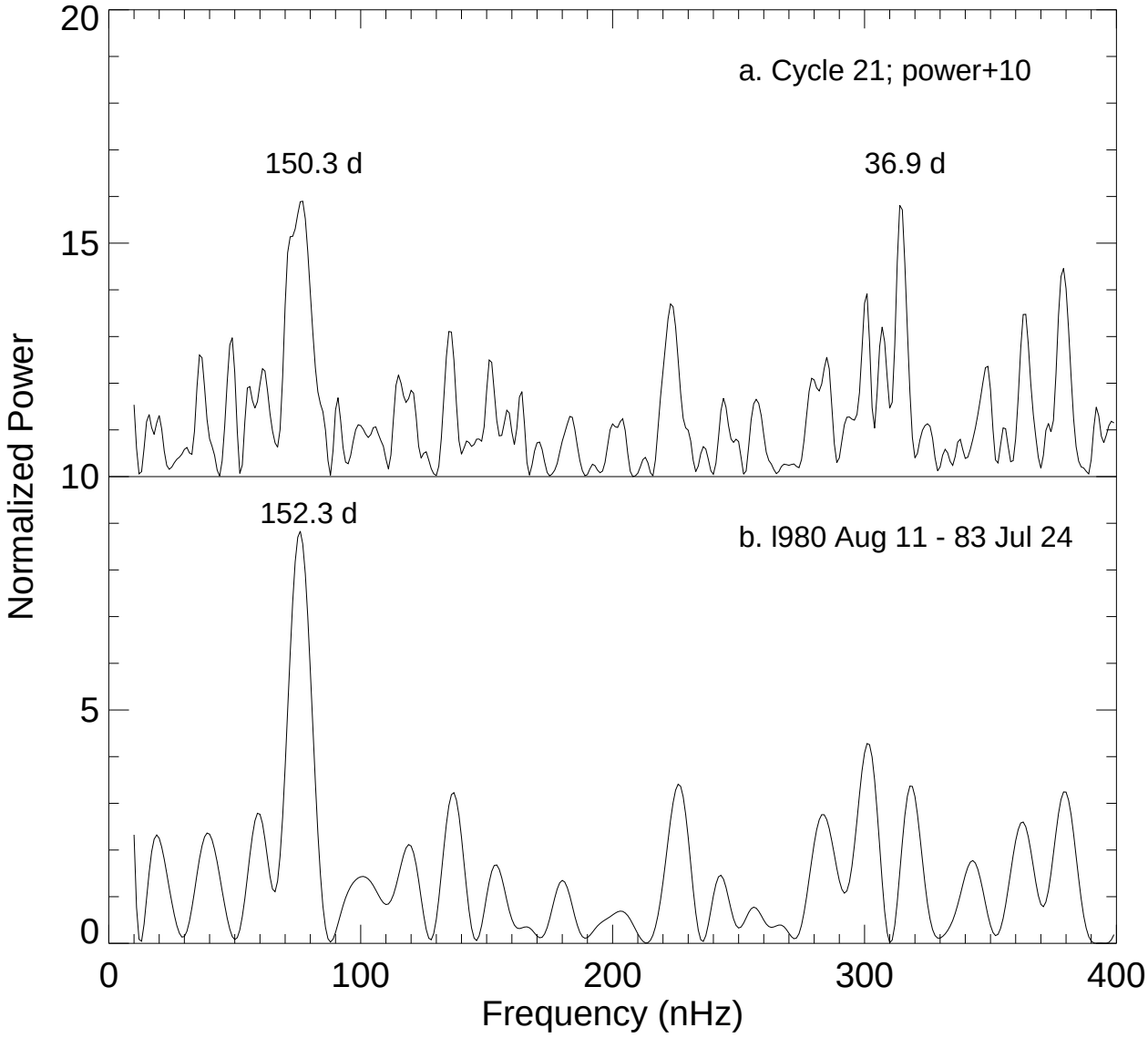

Fig. 11.— Longitude distribution for northern-hemisphere flares of cycle 21 for $P = 27.0\ d$.

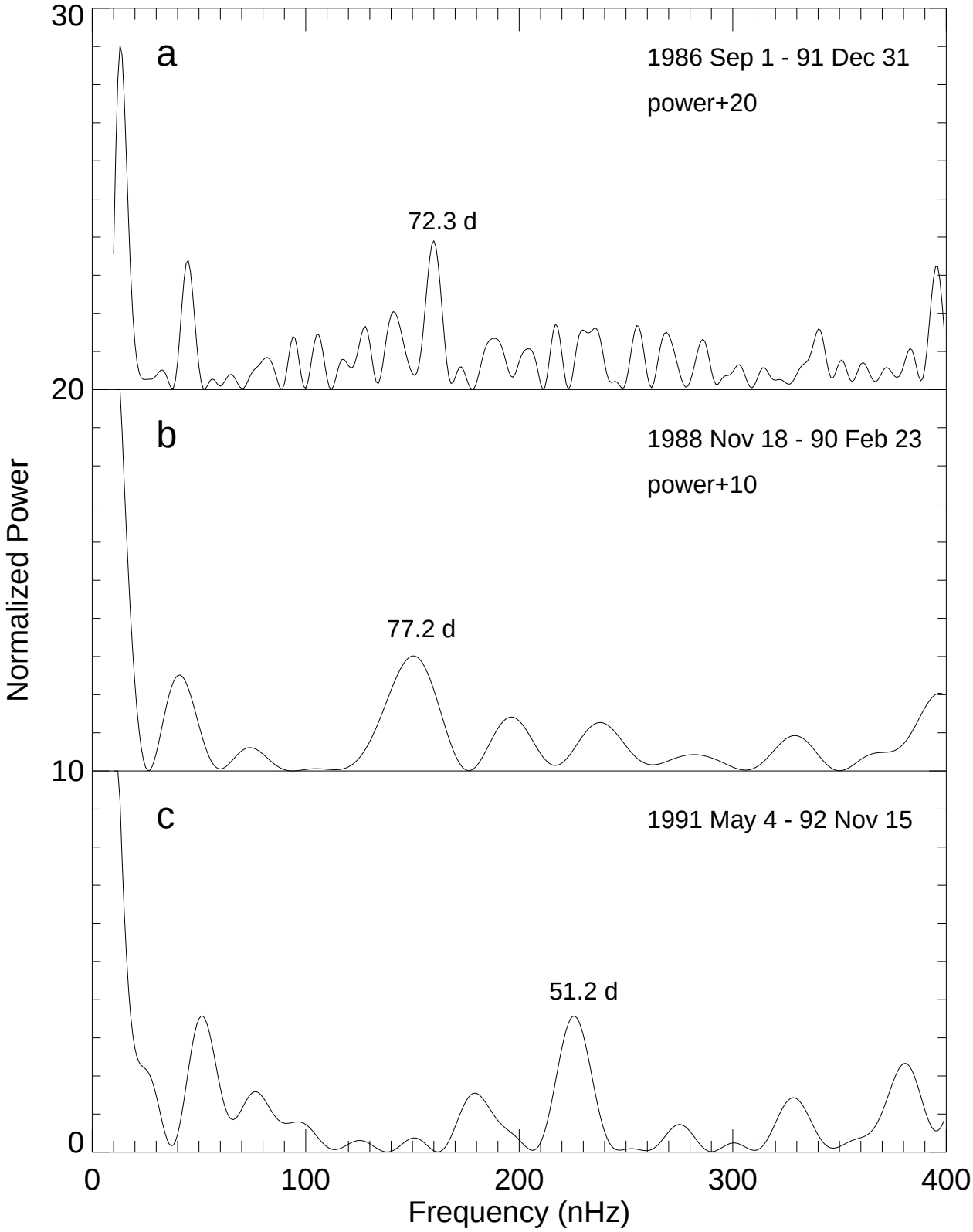

Fig. 12.— Longitude distributions for northern-hemisphere flares of cycles 20–22 for $P = 26.73\ d$. Baselines for the upper two panels are $y = 200$ and $y = 100$.

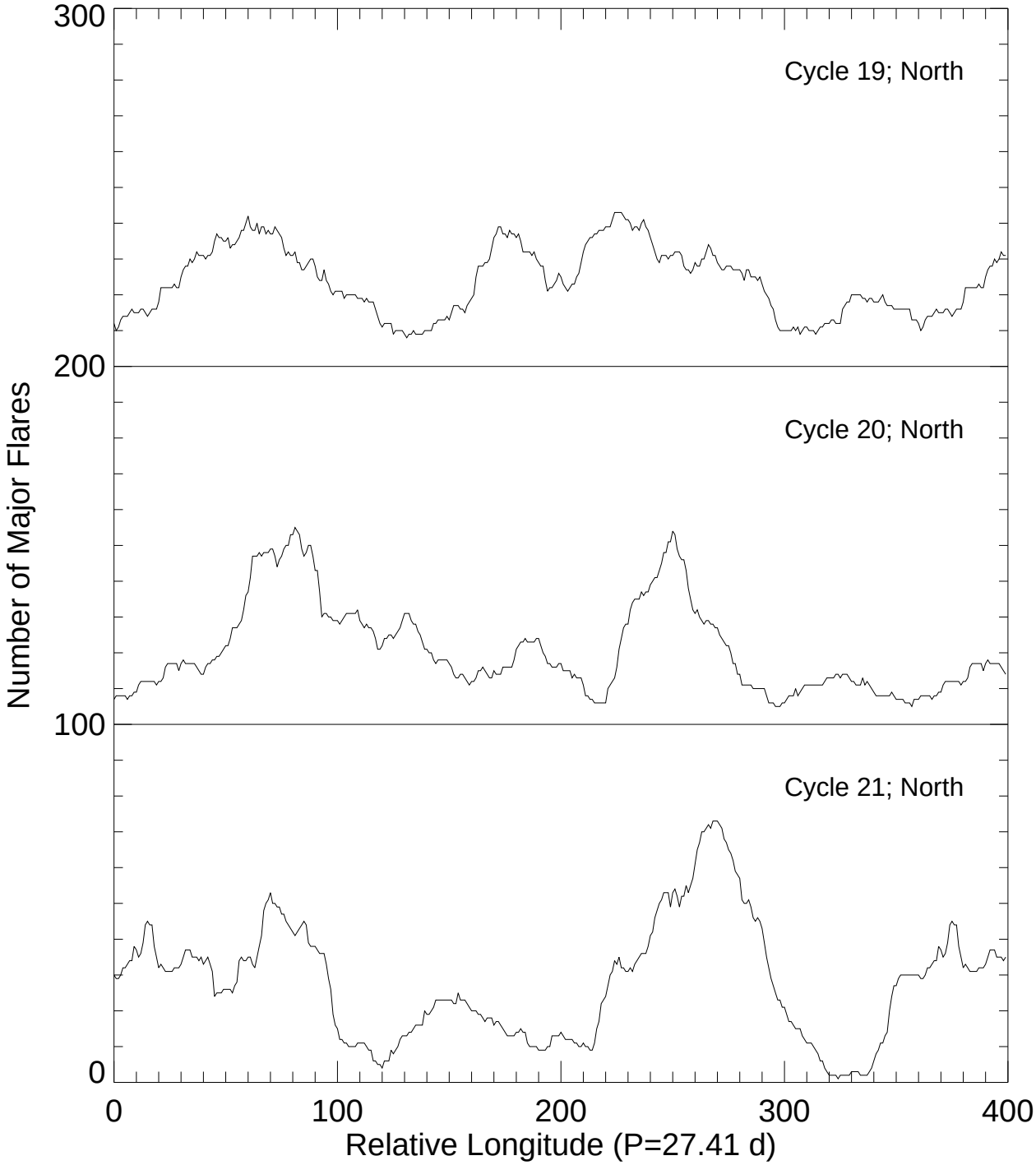

Fig. 13.— Longitude distributions for northern-hemisphere flares of cycles 19–21 for $P = 27.41\ d$. Baselines for the upper two panels are $y = 200$ and $y = 100$.

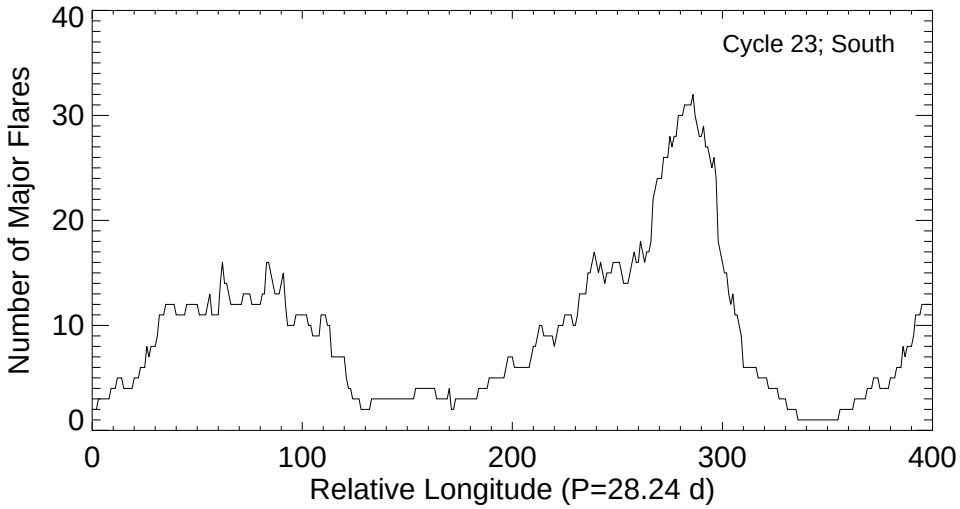

Fig. 14.— Longitude distribution for southern-hemisphere flares of cycle 23 for $P = 28.24\ d$.